The influence of mechanical grinding on the microstructure and corrosion behaviour of A356 aluminium alloys

M.D. Goodall[a], S. Pawar[a], M. Curioni[a], S. Morsch[a], M.G. Unthank[b,c], S.R. Gibbon[b] and X. Zhou[a*]

[a] *Corrosion and Protection Centre, Department of Materials, The University of Manchester, Manchester, M13 9PL*

[b] *AkzoNobel, Stoneygate Lane, Felling, Gateshead, Tyne & Wear, NE10 0JY, UK*

[c] *Northumbria University. Department of Applied Sciences, Faculty of Health and Life Sciences, Newcastle upon Tyne, NE1 8ST, UK*

* *Corresponding author, telephone: 01613064832, e-mail address: xiaorong.zhou@manchester.ac.uk*

Abstract

In the automotive industry, mechanical grinding is employed at finishing line rectification to remove defects left over from upstream, which may also result in microstructure modification within the near-surface region of the work piece and, consequently, affects its corrosion performance. The present work investigates the influence of mechanical grinding on the microstructure modification and corrosion behaviour of Al-Si-Mg (A356) alloy castings in order to advance the understanding of potential corrosion issues. It is found that a near-surface deformed layer with a maximum thickness of 3 μm, characterised by ultrafine equiaxed grains of 50-150 nm diameter, is introduced by the grinding process on α-aluminium matrix. The near-surface deformed layer has a significant impact on the corrosion behaviour of the alloy; specifically, preferential dissolution of the near-surface deformed layer occurs when exposed to NaCl solution, together with trenching of the aluminium matrix around the eutectic silicon particles.

Key Words

Al-Si-Mg alloy; Near-Surface Deformed Layer; Corrosion; Grain Refinement; Alloy Wheels

1. Introduction

Mechanical grinding, machining or rolling of metals involves significant frictional force between the toll and the work piece, which imposes a high level of shear strain into the near-surface region of the work piece. For aluminium alloys, such shear strain are of sufficient magnitude to cause geometric dynamic recrystallization, resulting in grain refinement within the near-surface region and, consequently, the formation of a near-surface deformed layer (NSDL) [1]. The near-surface deformed layer is characterised by ultrafine equiaxed grains, accumulation of oxides and segregation of alloying elements at grain boundaries [2–16]. Previous work show that near-surface deformed layer has significant influence on optical [17,18], tribological [19,20] and corrosion [7–9,11-13,21-24] properties. The near-surface deformed layer formed on wrought aluminium alloys generally shows high susceptibility to filiform/cosmetic corrosion, due to various factors including preferential precipitation and segregation of alloying elements at grain boundaries, increased grain stored energy caused by residual strain, and increased population density of grain boundary [3-6, 11-13, 25-27]. For example, Liu et al [5] reported that the high corrosion susceptibility of a near-surface deformed layer introduced on AA6111-T4 alloys by mechanical grinding is due to the preferential precipitation of fine Q phase ($Cu_2Mg_8Si_7Al_4$) particles at the grain boundaries within the near-surface deformed layer since the microgalvanic coupling between the Q phase precipitates and the aluminium matrix adjacent to the particles provides the driving force for intergranular corrosion. Similarly, Liu et al [9] found that the high corrosion susceptibility of machined AA7150-T651 aluminium alloy is due to the preferential anodic dissolution of grain boundaries within the near-surface deformed layer where grain boundary segregation of magnesium and zinc occurs during machining.

The high filiform/cosmetic corrosion susceptibility of the near-surface deformed layer on aluminium alloys is of significant relevance to the automotive industry as aluminium alloys are increasingly used for vehicle body structure and alloy wheels with the aim of reducing vehicle weight and, consequently, reducing CO_2 emission. Alloy wheels are mostly made of A356 cast aluminium alloy. In alloy wheel production, surface finishing operations including machining and mechanical grinding are carried out to enhance appearance. Machining is employed to generate the ‘diamond cut’ finish and mechanical grinding is used to remove small burrs and defects left over from casting stage [28]. As described above, such operations can introduce a near-surface deformed layer to wrought aluminium alloys. However, A356 cast alloy consists of primary α-aluminium and eutectic regions, which is different from previous work on the

near-surface deformed layer formed on wrought aluminium alloys. Thus, the formation of near-surface deformed layer on A356 cast alloy and its influence on corrosion property might be different, particularly within the eutectic regions where a relatively high volume fraction of hard and brittle silicon phase is present, which is difficult to be deformed and has different electrochemical property from α-aluminium. In the present study, the effect of mechanical grinding on the microstructure in the near-surface region of A356 cast aluminium alloy and its influence on the corrosion behaviour of the alloy are investigated, with a focus on comparing the microstructure modification and the associated corrosion behaviour in primary α-aluminium and eutectic regions.

2. Experimental

A commercial A356 aluminium alloy (7Si, 0.35Mg, 0.2Fe, 0.2Mn, 0.1Zn, 0.1Ti, 0.015Sr, bal. Al wt%) in the form of cast panels in T6 temper was employed in the present study. Following the standard industry practice, the panels were mechanically ground with 120 grit silicon carbide paper without lubricant for 5 minutes at 200 revolutions per minute (rpm). The prepared surfaces were then cleaned with ethanol, washed with deionised water and dried in a cool air stream.

Characterisation of the near-surface region was performed using transmission electron microscopy (TEM) on an FEI Tecnai G^2 T20 instrument operating at an accelerating voltage of 200 kV. TEM was performed on the cross sections that were prepared from the near-surface region using a diamond knife on a Leica Ultracut ultramicrotome. The ultramicrotomed sections were collected using 400 mesh nickel grids. A Zeiss Ultra55 field emission gun scanning electron microscope, equipped with Oxford Instruments energy dispersive X-ray (EDX) analysis system, was employed to examine the near-surface region of the mechanically ground alloy in both plan view and in cross section. An accelerating voltage of 5 kV was employed to control the interaction volume and to optimize surface sensitivity for the characterizing of the near-surface region using both secondary (SE) and backscattered electron (BSE) detectors. For cross sectional examination by scanning electron microscopy (SEM), the samples were prepared using ultramicrotomy under dry condition.

Scanning Kelvin probe force microscopy (SKPFM) was performed on the mechanically polished sample to obtain the Volta potential of the individual phases present in the alloy on a

Veeco Dimension 3100 atomic force microscope, using PtIr-coated Si tip with a nominal tip radius of 15 nm, spring constant of 0.5–4.4 N m−1 and resonant frequency of 45–95 kHz. The Volta potential maps were produced at a resolution of 512 x 512 pixels in a 75 x 75μm area and scan frequency of 0.2 Hz. The open circuit potential of the variously prepared surfaces was recorded when the specimens were immersed in 3.5 wt.% sodium chloride solution at 30°C for 6 hours. Post corrosion characterisation was conducted on the specimens after the immersion testing.

3. Results

3.1 The microstructure of A356 aluminium alloy cast coupons

Fig. 1 shows a scanning electron micrograph of the A356 aluminium alloy cast coupon. The prominent phase is the primary α-aluminium which forms the matrix of the alloy. The regions between the primary α-aluminium are the eutectic regions consisting of eutectic silicon and eutectic α-Al phase, as indicated by the dashed line frame. The other phase revealed in the micrograph is the bright plate-like intermetallic particles, as indicated by the arrows. EDX analysis confirmed that the plate-like particles are AlFeSi intermetallics.

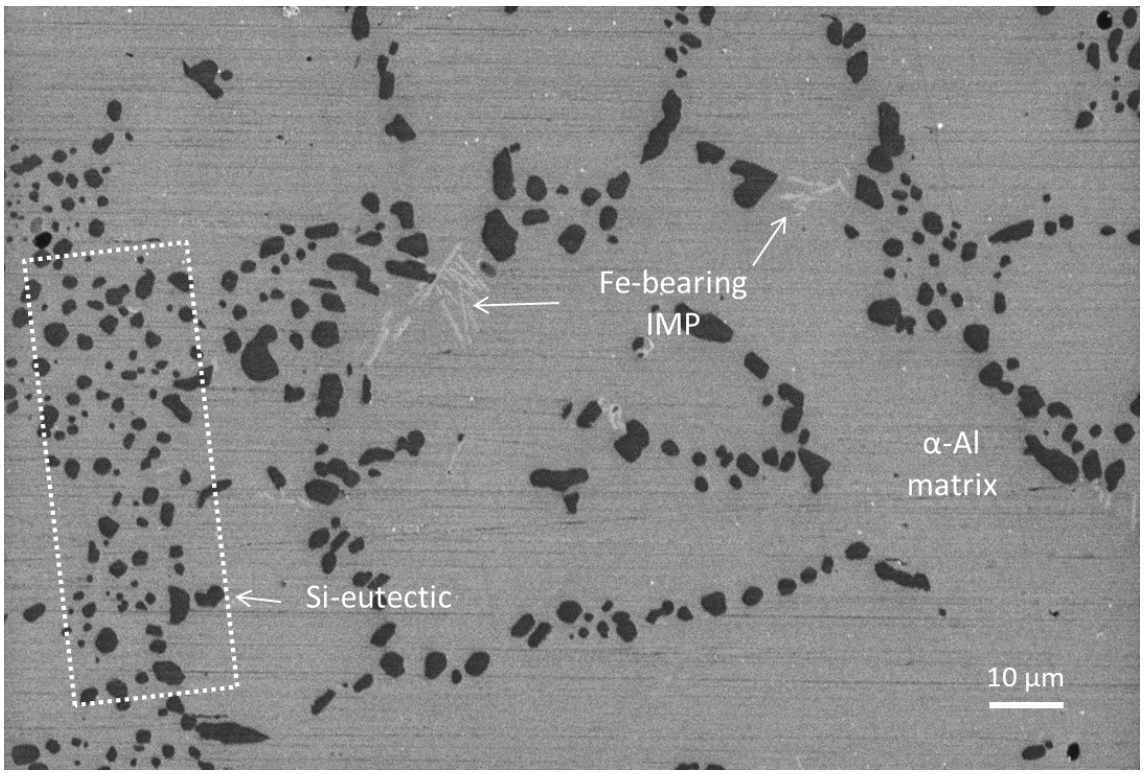

Fig.1 Scanning electron micrograph of the A356 cast aluminium alloy.

SKPFM was performed on the eutectic phases, as shown in Fig. 2. It is evident that silicon eutectic particles exhibit more positive potential relative to α-aluminium matrix. The Volta potential profile across three adjacent silicon particles in the eutectic region reveals a potential difference of about 200 mV between the silicon particles and the surrounding α-aluminium matrix, consistent with previous work on similar alloy microstructures [29].

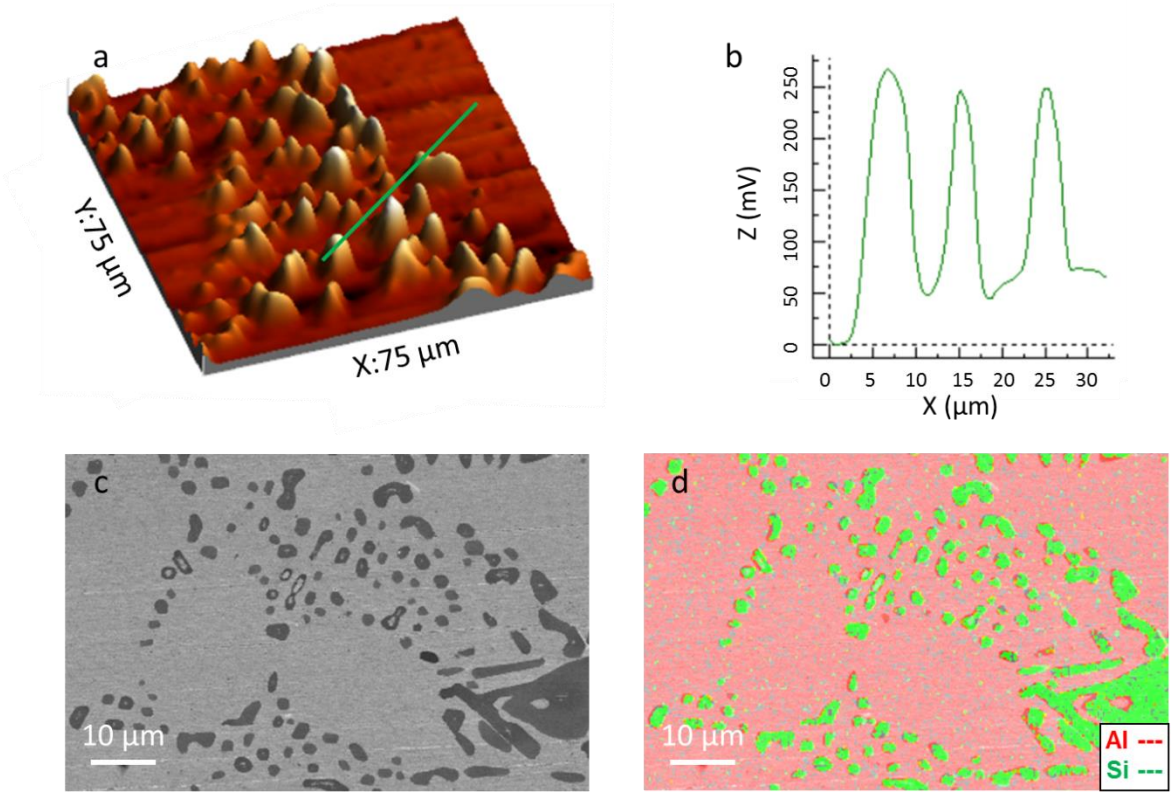

Fig.2 (a) 3D Volta potential map of the Al-Si-eutectic region in the A356 cast aluminium alloy; (b) corresponding Volta potential line scan indicated the green line in (a), showing a Volta potential difference of ~200 mV between individual Si particles and the α-Al matrix; (c) scanning electron micrograph of a Al-Si-eutectic region in the A356 cast aluminium alloy; and (d) the corresponding aluminium and silicon EDX map.

3.2 Near-surface deformed layer on mechanically ground A356 aluminium alloy

The scanning electron micrograph of the mechanically ground alloy surface is displayed in Fig. 3, revealing clearly the grinding tracks. Further, ultrafine equiaxed grains, with a diametre of less than 100 nm, are clearly shown by the channelling contrast. In order to determine the thickness of the near-surface deformed layer and to examine the fine-grained structure in more

detail, scanning and transmission electron microscopy were performed on the ultramicrotomed cross section of the near-surface region, as shown in Fig. 4.

Fig.3 Scanning electron micrograph of the mechanically ground A356 aluminium alloy surface.

Fig. 4a reveals clearly a near-surface deformed layer characterized by ultrafine, equiaxed grains. A clear transition between the near-surface deformed layer and the bulk alloy is observed, as indicated by the dashed line. It is evident that the grain size varies through the NSDL with grains in the range of 50-75 nm observed at the outer region and up to 100 nm observed at the inner region. The thickness of the NSDL is approximately 1.7 μm and is relatively uniform across the section examined. It is also evident in Fig.4b that the grain boundaries are free from oxide particles, different from the NSDL formed during rolling [1].

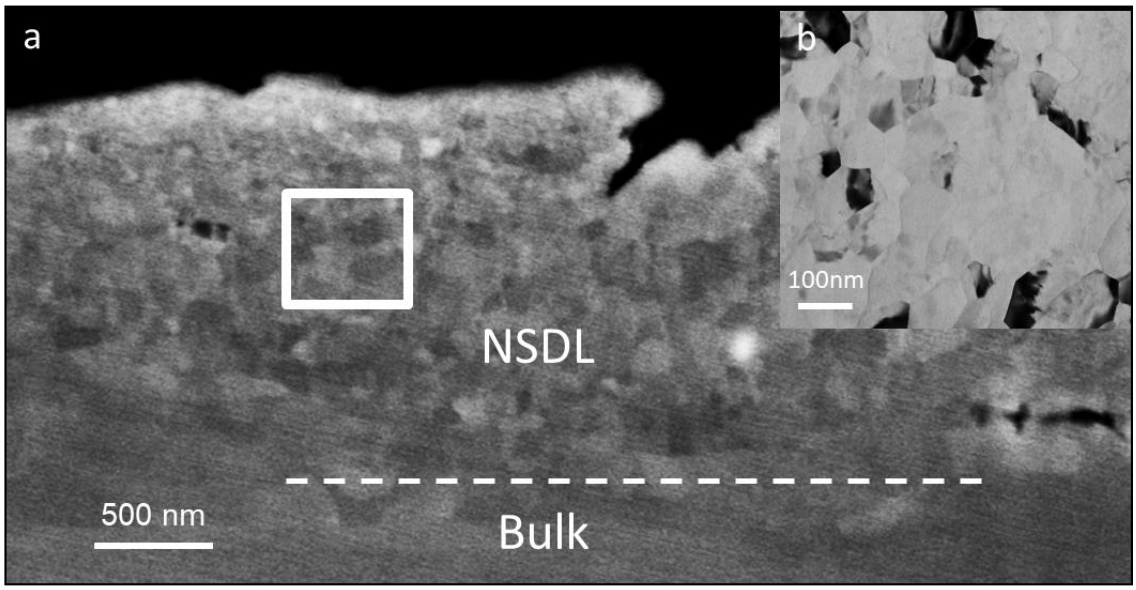

Fig.4 (a) Scanning electron micrograph of a cross section showing the near-surface deformed layer (NSDL) on the mechanically ground alloy; and (b) a bright-field transmission electron micrograph showing the ultrafine grains from the region indicated by the frame in (a).

Fig. 5a displays a secondary electron image of a eutectic region on the mechanically ground alloy surface, appearing as being disrupted by a particle. The EDX map shown in Fig. 5b confirms that the particle is silicon. The eutectic silicon particle also appears to be fractured by the grinding process due to their brittleness.

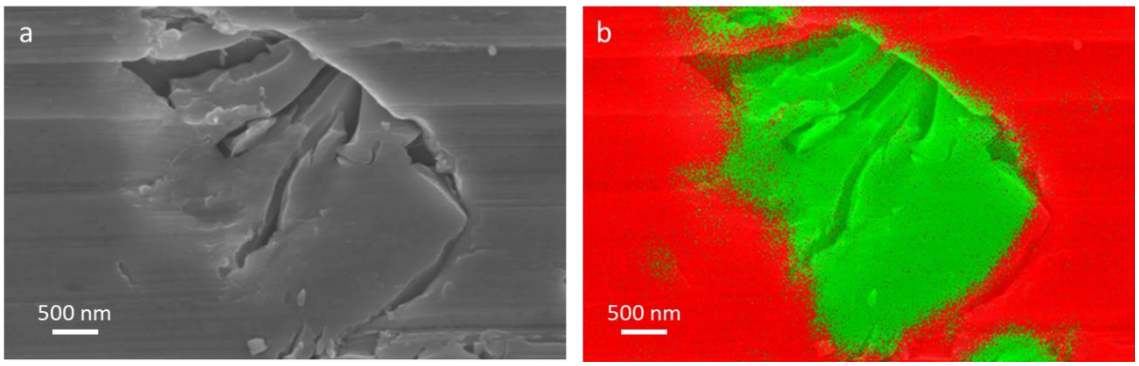

Fig.5 (a) Secondary electron image showing a silicon particle on the mechanically ground alloy surface; and (b) the corresponding EDX map.

Fig. 6a shows a scanning electron micrograph of the cross section taken from a eutectic region on the mechanically ground A356 alloy. It is evident that an individual silicon particle intersects the surface whilst a few more silicon particles remain buried. It can be seen that the

ultrafine equiaxed grains that are characteristic of near-surface deformed layers are absent above the silicon particle, whereas a NSDL of 2 - 3μm thickness is present on α-Al matrix. Fig. 6b shows a SEM image at increased magnification at one of the shallowly buried silicon particles highlighted by the red dashed line circle. The dark features in the silicon particle are cracks introduced by diamond knife cutting during preparing the cross section in ultramicrotome since silicon is hard and brittle. The particle is buried just below the surface. Interestingly, a relatively thin near-surface deformed layer is present above the particle. Fig. 6b also reveals the plastic flow pattern of α-aluminium matrix around the silicon particle, as indicated by the yellow dashed line. Microbands of elongated grains aligned parallel to the surface are also evident at the interface between the near-surface deformed layer and the bulk alloy. The presence of the bands in the inner region and the ultrafine equiaxed grains in the outer region indicate that the plastic strain levels at different depths from the surface are different, with greater strain introduced in the regions closer to the surface. This is consistent with previous study on the formation of near-surface deformed layer during rolling of aluminium alloys [1].

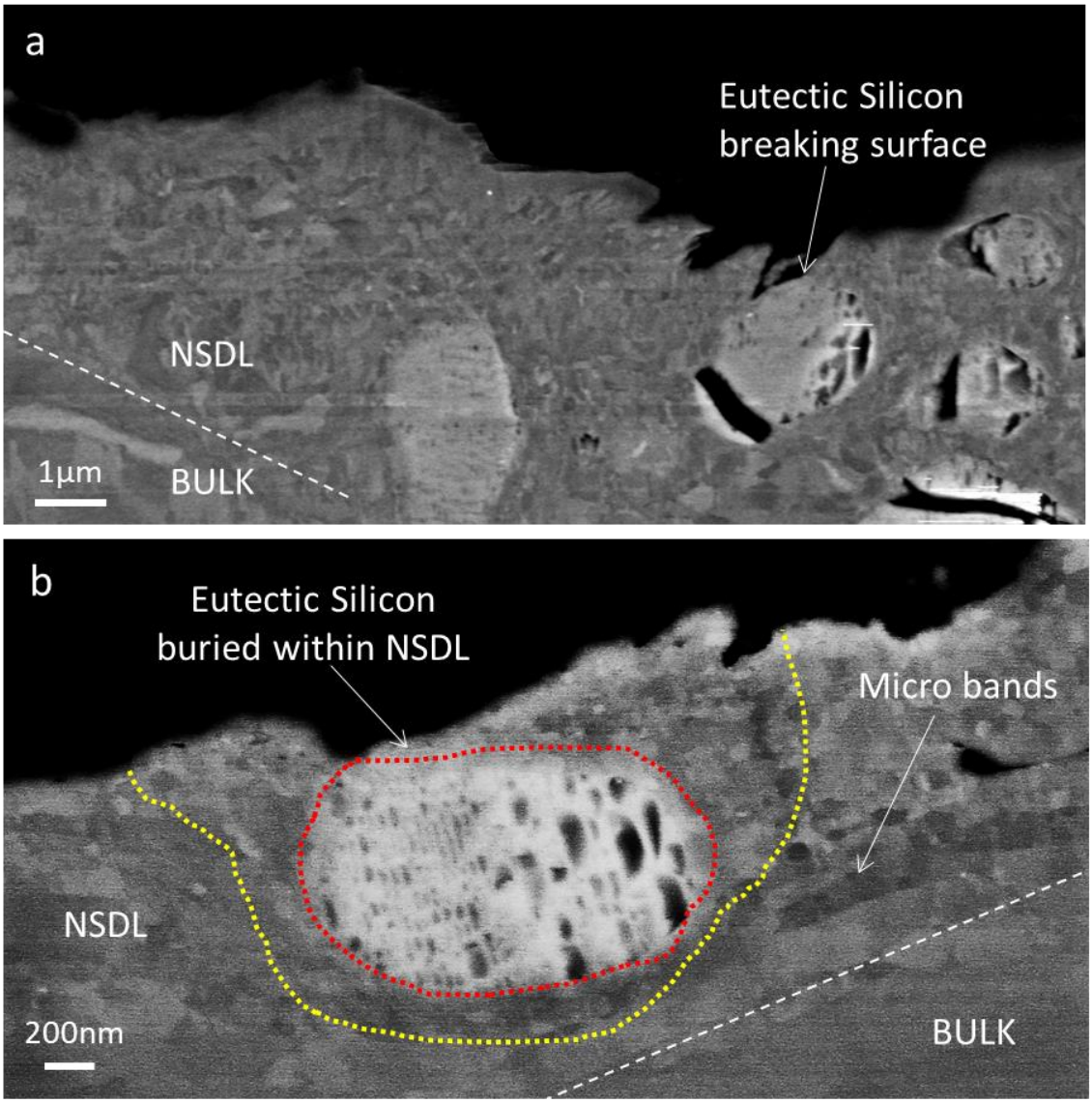

Fig.6 Scanning electron micrographs of an ultramicrotomed cross section taken from a eutectic region on the mechanically ground A356 alloy.

3.3 Corrosion behaviour of mechanically ground A356 aluminium alloy

The corrosion behaviour of the mechanically ground A356 aluminium alloy was investigated by immersion testing in 3.5 wt.% sodium chloride solution. During the testing, the open circuit potential (OCP) of the alloy was measured, as shown in Fig.7. At the beginning of immersion, a potential transient, consisting of an initial drop followed by a gradual increase, is clearly evident. After the minimum of -1.05 V (SCE), the OCP progressively increased to -0.82 V (SCE).

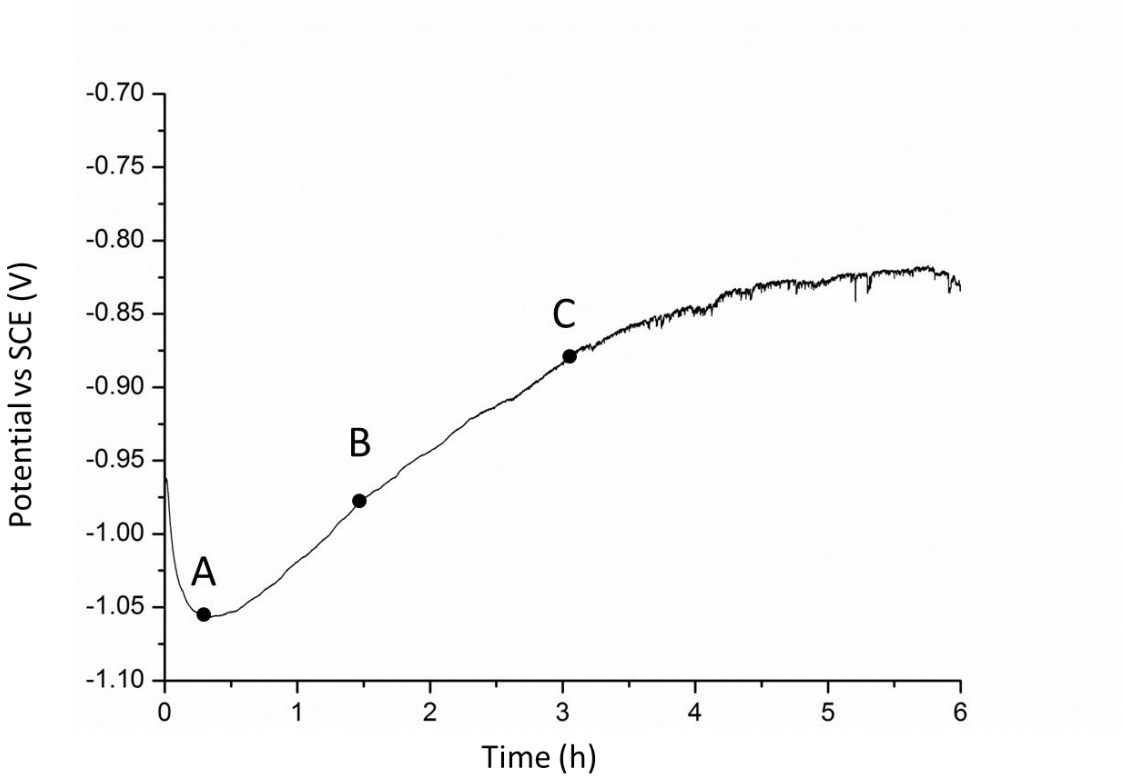

Fig.7 Open circuit potential-time response of the mechanically ground A356 aluminium alloy in 3.5 wt.% NaCl solution.

In order to verify whether or not the OCP transient is related to the near-surface deformed layer and to gain an insight into the corrosion behaviour of the mechanically ground A356 alloy, specimens were removed at specific times indicated with A, B and C on the OCP-time curve shown in Fig. 7 and subjected to microscopic examination. Fig. 8 shows a scanning electron micrograph of the specimen removed at point A indicated in Fig. 7. The mechanical grinding tracks and fractured silicon particles are clearly revealed. Fig. 8 also reveals clearly pit-like features, as indicated by the arrow. The size of the pit-like features is in the range of 50-100 nm, consistent with the grain size in the near-surface deformed layer. Comparing Fig. 8 with Fig. 3, i.e. the primary α-aluminium region before and after immersion, it is evident that the pit-like features revealed in Fig. 8 is associated with local dissolution of the near-surface deformed layer, indicating that corrosion of the NSDL had started on the surface.

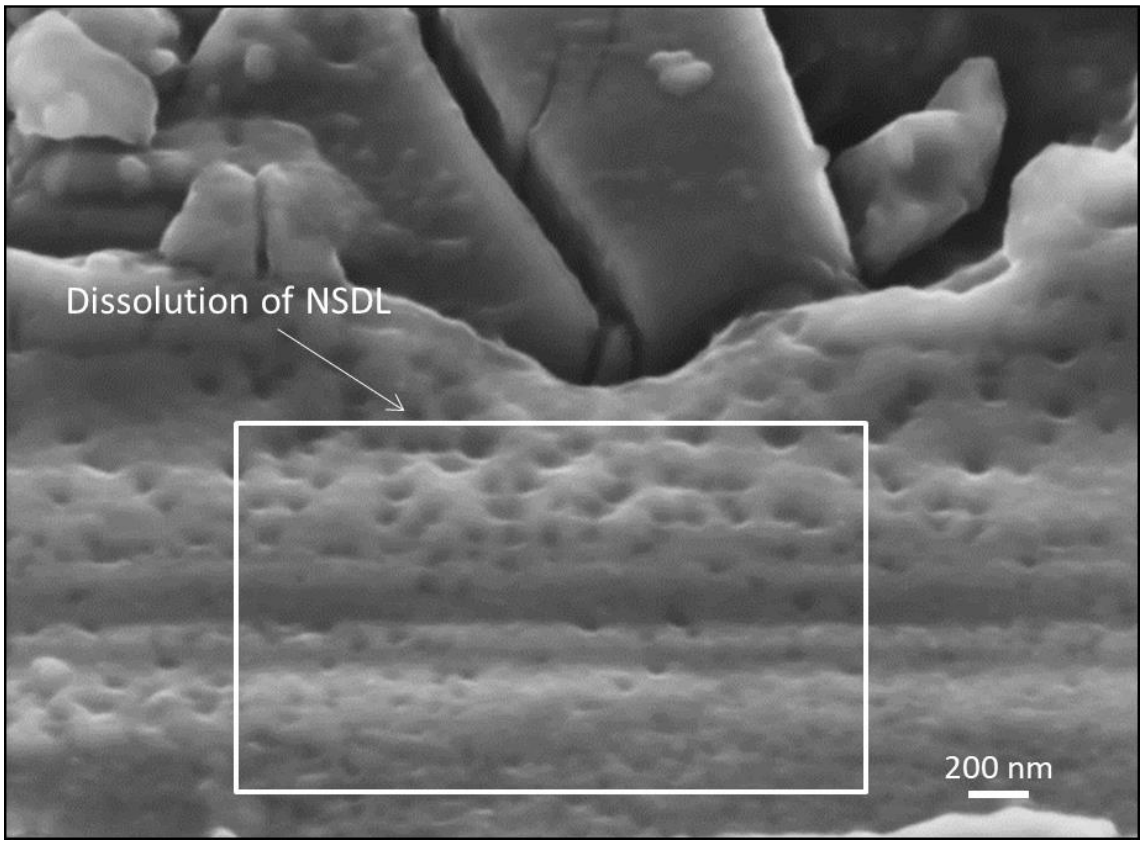

Fig.8 Scanning electron micrograph of the mechanically ground A356 alloy after immersion in 3.5 wt.% NaCl solution until point A indicated in Fig. 7.

A scanning electron micrograph of the specimen removed at point B indicated in Fig. 7 is shown in Fig. 9a, revealing patches of cavities associated with the dissolution of the near-surface deformed layer within the primary α-aluminium region, as indicated by the arrows. Further, Fig. 9b shows a localised corrosion site within the eutectic region, revealing trenching of the aluminium matrix around a silicon particle intersecting the alloy surface. This is confirmed in the EDX map shown in Fig. 9c as increased oxygen yields were detected around the silicon particle, indicating the corrosion products associated with the trenching of aluminium matrix.

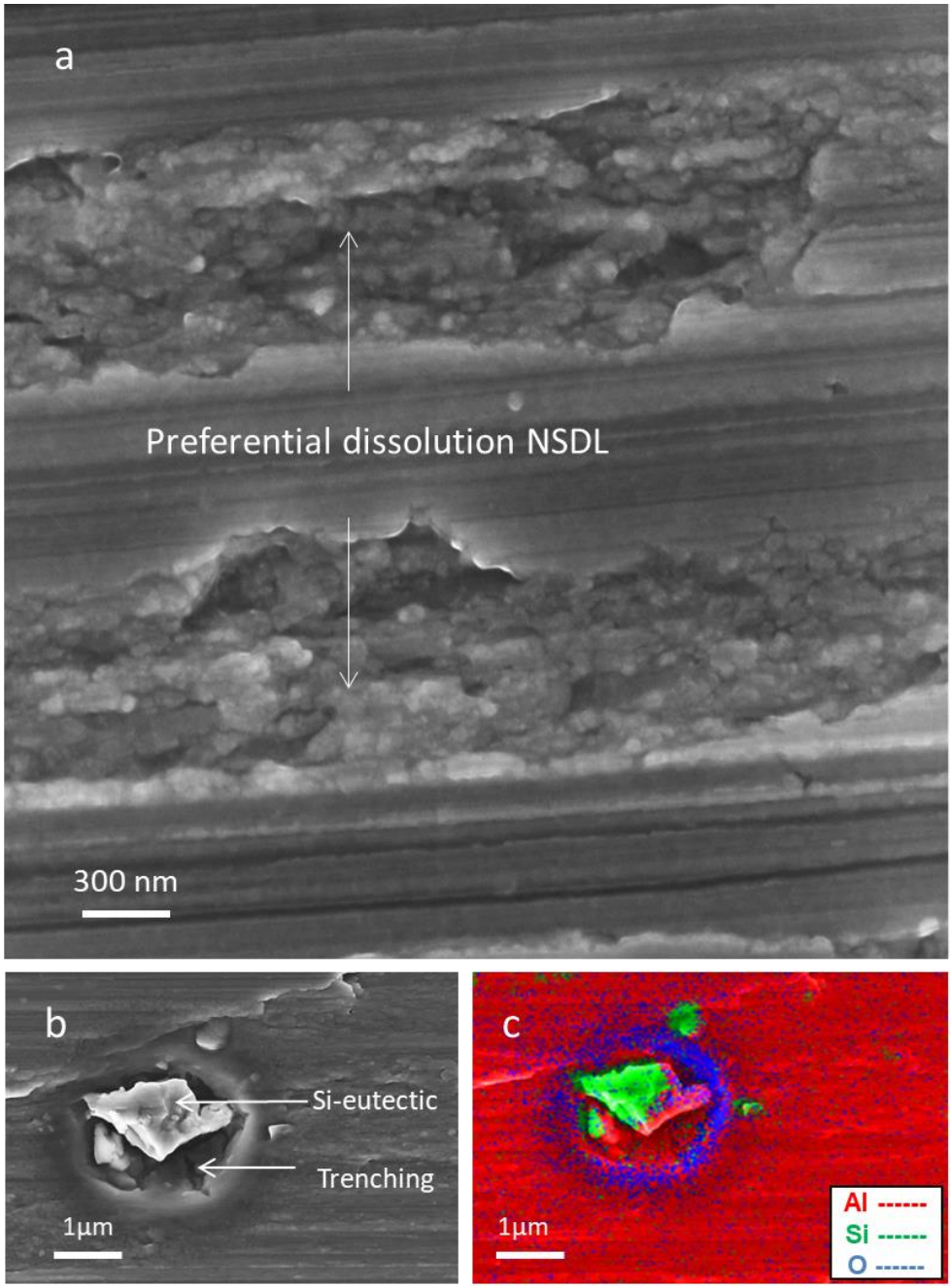

Fig.9 (a)-(b) Scanning electron micrographs of the mechanically ground A356 alloy after immersion in 3.5 wt.% NaCl solution until point B indicated in Fig. 7; and (c) EDX map corresponding to the area shown in (b).

The influence of silicon particles on the corrosion behaviour of the A356 alloy is also evident on the specimen removed at point C indicated in Fig. 7. Figs. 10a and c show that trenching of the aluminium matrix around individual silicon particles that intersect the surface has further developed. EDX maps shown in Figs.10b and d exhibit increased oxygen yields associated with corrosion products. The preferential dissolution of alloy matrix around the silicon particles at point C may lead to pitting in the bulk alloy, which is evidenced by the open circuit potential-time response (Fig.7) that exhibits potential oscillations typical of pitting after point C.

Although the EDX maps in Figs.10b and d reveal a number of silicon particles, localised corrosion has only developed at 3 particles that intersect the surface, but not in the vicinity of those particles that remain buried beneath the surface (buried particles are visible in the EDX map since, with 10kV accelerating voltage, X-ray is generated from a volume up to 1 micron depth below the surface).

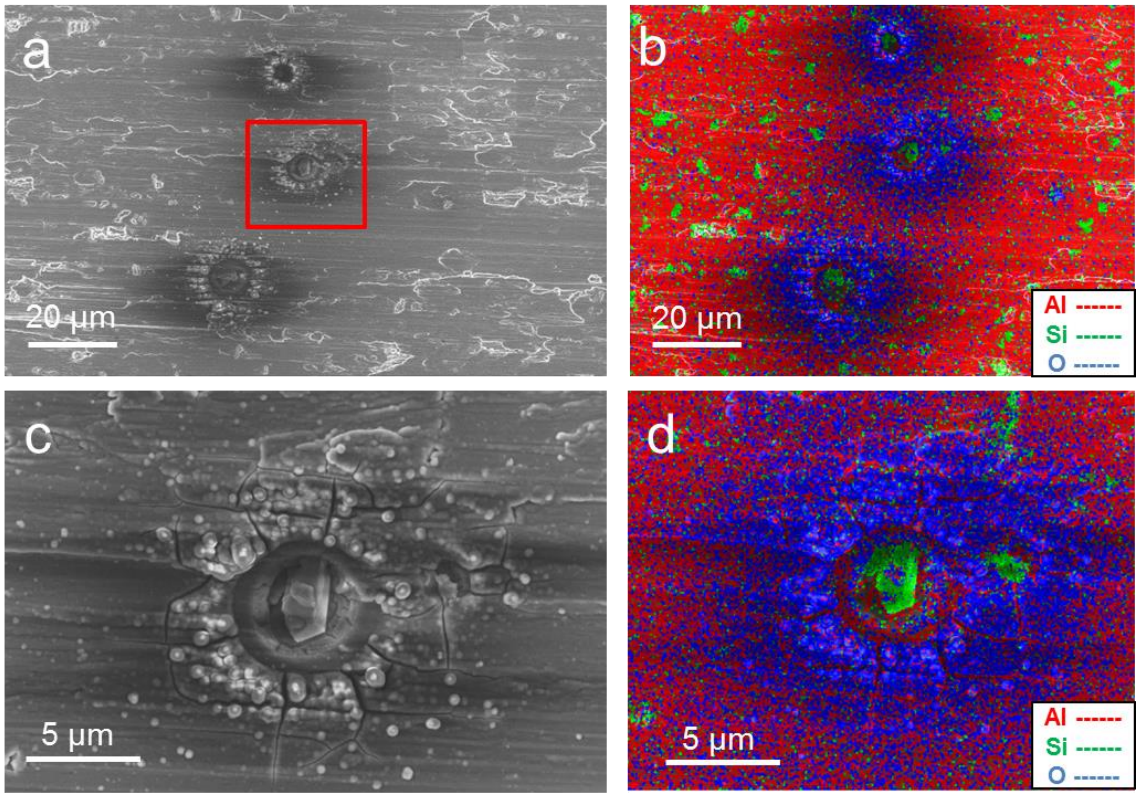

Fig.10 (a) Scanning electron micrograph of the mechanically ground A356 alloy after immersion in 3.5 wt.% NaCl solution until point C indicated in Fig. 7; (b) corresponding EDX map of the area shown in (a); (c) the region indicated by the frame in (a) at an increased magnification and (d) the corresponding EDX map.

4. Discussion

4.1 Near-surface deformed layer on mechanically ground A356 aluminium alloy

It is now well known that near-surface deformed layer is formed during severe strain processing of wrought aluminium alloys [1-16]. When significant amounts of plastic strain are introduced into the alloy, grain refinement can take place through dynamic recrystallization [1]. Aluminium has high stacking fault energy, which tends to promote the formation of sub-grains. As deformation continues the grains flatten and serrated grain boundaries come together, with

the sub-grain size remaining constant. When the thickness of the grain has become comparable with the size of the serrations, impingement of the grain boundary occurs, resulting in a microstructure of ultrafine equiaxed grains. This concept is termed geometric dynamic recrystallization (GDRX) [30], which is responsible for the grain refinement in near-surface deformed layer on the α-aluminium regions in the A356 alloy.

However, the situation at the surface of A356 cast aluminium alloy is different from that of a wrought alloy. In addition to the formation of a fine, equiaxed grain structure on the α-aluminium regions, discontinuity of the near-surface deformed layer is introduced by the presence of eutectic silicon particles in the alloy. The eutectic silicon particles are significantly harder than the surrounding aluminium matrix. During mechanical grinding, these particles do not deform plastically, unlike α-aluminium matrix. Therefore, if a eutectic silicon particle is situated on or near the surface of the alloy, a near-surface deformed layer would either not be formed or would be limited within α-aluminium matrix above the eutectic silicon particle, as shown in Figs. 5 and 6.

Therefore, the mechanically ground A356 cast alloy surface has two distinct regions: Region 1, where there is a near-surface deformed layer formed on primary α-aluminium matrix; and Region 2, where the near-surface deformed layer is interrupted by the eutectic silicon particles present at the alloy surface.

4.2 Corrosion behaviour of mechanically ground A356 aluminium alloy

The open circuit potential-time response of the mechanically ground alloy in 3.5 wt.% NaCl solution (Fig.7) shows potential transient at the beginning of immersion, which is due to the preferential dissolution of the NSDL under the test conditions (Figs 8 and 9). The near-surface deformed layer has a high volume-fraction of grain boundaries which are anodically active, thus, resulting in a more negative initial value of corrosion potential. Further, it is known that plastically deformed grains with a high dislocation density and therefore a large stored energy are also anodically active [31]. Thus, the plastic strain introduced by the grinding process can also increase the anodic activity of the near-surface deformed layer, resulting in a more negative initial value of corrosion potential. As revealed in Figs 8 and 9, the anodically active near-surface deformed layer is preferentially dissolved when the mechanically ground alloy is exposed to the testing solution. Interestingly, as revealed in Fig. 9a, the preferential dissolution of the near-surface deformed layer occurred in bands intercalated by intact regions. The non-uniform dissolution of the near-surface deformed layer in some regions is due to local

breakdown of air-formed surface alumina film. The local breakdown of surface film preferentially occurs at defects. Subsequently, anodic dissolution of the near-surface deformed layer initiates at the regions where local breakdown of surface film has occurred. With the progressive dissolution of the near-surface deformed layer, its area percentage on the specimen surface decreases progressively, leading to the progressive increasing of the OCP until the near-surface deformed layer is completely dissolved and the OCP is stabilised at the value for the bulk alloy. Since the potential of the bulk alloy is higher than that of the near-surface deformed layer, during the process of preferential dissolution of the near-surface deformed layer, corrosion was confined within the near-surface deformed layer without developing further into the bulk alloy. In other words, galvanic coupling is formed between the near-surface deformed layer and the bulk alloy beneath, with the latter being cathodically protected [9].

However, the preferential dissolution is not the only form of corrosion that occurs on the surface of the mechanically ground A356 alloy during immersion. As revealed in Figs. 9 and 10, trenching around the eutectic silicon particles also occur, which is due to the combined effect of severe plastic strain of the aluminium matrix in the periphery of the silicon particles (Fig 6b) and the galvanic coupling between the cathodically active silicon particles and the anodically active aluminium matrix since the silicon eutectic particles are approximately 200 mV noble than the aluminium matrix.

Therefore, both preferential dissolution of the near-surface layer and localized corrosion around silicon particles that are intersect the surface occur simultaneously on the mechanically ground A356 alloy surface. This has significant consequences for the filiform/cosmetic corrosion susceptibility of coated aluminium alloys wheels since filiform corrosion can be categorised into two types: fast filiform corrosion linked to the attack of a near-surface deformed layer; and slow filiform corrosion, which progresses due to pitting and subsequent blistering of the coating in the periphery of pit [6].

5. Conclusions

Mechanical grinding introduces a dual-region microstructure into the near-surface region of A356 aluminium alloy. The first region contains a continuous near-surface deformed layer on the primary α-aluminium areas, comprised of characteristic ultrafine equiaxed grains with size varying from 50-75 nm in the outmost region to 100-150 nm in the inner region. The other

region is over eutectic α-aluminium and silicon, with a near-surface deformed layer that is disrupted in the areas where silicon particles intersect the surface.

Preferential dissolution of the near-surface deformed layer and trenching of aluminium matrix around eutectic silicon particles occur simultaneously when the mechanically ground A356 alloy is exposed to NaCl solution. Such corrosion behaviour implies that mechanical grinding of A356 aluminium alloy may increase filiform corrosion susceptibility of the alloy.

Acknowledgements

The authors wish to thank the UK Engineering and Physical Sciences Research Council (EPSRC) for the provision of financial support for the Advanced Metallics Systems Centre for Doctoral Training (EP/G036950) and SusCoRD Prosperity Partnership Grant (EP/S004963/1), and AkzoNobel for provision of financial support and the materials used in this research. All research data supporting this publication are directly available within this publication.

References

[1] X. Zhou, Y. Liu, G.E. Thompson, G.M. Scamans, P. Skeldon, J.A. Hunter, Near-surface deformed layers on rolled aluminum alloys, Metall. Mater. Trans. A Phys. Metall. Mater. Sci. 42 (2011) 1373–1385. doi:10.1007/s11661-010-0538-2.

[2] G.M. Scamans, M.F. Frolish, W.M. Rainforth, Z. Zhou, Y. Liu, X. Zhou, G.E. Thompson, The ubiquitous beilby layer on aluminium surfaces, Surf. Interface Anal. 42 (2010) 175–179. doi:10.1002/sia.3204.

[3] Y. Liu, A. Laurino, T. Hashimoto, X. Zhou, P. Skeldon, G.E. Thompson, G.M. Scamans, C. Blanc, W.M. Rainforth, M.F. Frolish, Corrosion behaviour of mechanically polished AA7075-T6 aluminium alloy, Surf. Interface Anal. 42 (2010) 185–188. doi:10.1002/sia.3136.

[4] H.N. McMurray, A. Holder, G. Williams, G.M. Scamans, A.J. Coleman, The kinetics and mechanisms of filiform corrosion on aluminium alloy AA6111, Electrochim. Acta.

55 (2010) 7843–7852. doi:10.1016/j.electacta.2010.04.035.

[5] Y. Liu, X. Zhou, G.E. Thompson, T. Hashimoto, G.M. Scamans, A. Afseth, Precipitation in an AA6111 aluminium alloy and cosmetic corrosion, Acta Mater. 55 (2007) 353–360. doi:10.1016/j.actamat.2006.08.025.

[6] X. Zhou, G.E. Thompson, G.M. Scamans, The influence of surface treatment on filiform corrosion resistance of painted aluminium alloy sheet, Corros. Sci. 45 (2003) 1767–1777. doi:10.1016/S0010-938X(03)00003-9.

[7] A. Afseth, J.H. Nordlien, G.M. Scamans, K. Nisancioglu, Influence of heat treatment and surface conditioning on filiform corrosion of aluminium alloys AA3005 and AA5754, Corros. Sci. 43 (2001) 2359–2377. doi:10.1016/S0010-938X(01)00019-1.

[8] A. Afseth, J.H. Nordlien, G.M. Scamans, K. Nisancioglu, Effect of heat treatment on filiform corrosion of aluminium alloy AA3005, Corros. Sci. 43 (2001) 2093–2109. doi:https://doi.org/10.1016/S0010-938X(01)00014-2.

[9] B. Liu, X. Zhang, X. Zhou, T. Hashimoto, J. Wang, The corrosion behaviour of machined AA7150-T651 aluminium alloy, Corros. Sci. 126 (2017) 265–271. doi:10.1016/j.corsci.2017.07.008.

[10] Y. Liu, M.F. Frolish, W.M. Rainforth, X. Zhou, G.E. Thompson, G.M. Scamans, J.A. Hunter, Evolution of near-surface deformed layers during hot rolling of AA3104 aluminium alloy, Surf. Interface Anal. 42 (2010) 180–184. doi:10.1002/sia.3135.

[11] Z. Zhao, G.S. Frankel, On the first breakdown in AA7075-T6, Corro. Sci. 49 (2007) 3064–3088.

[12] B. Liu, X. Zhou, The impact of machining on the corrosion behaviour of AA7150-T651 aluminium alloy, Mater. Sci. Forum 794 (2014) 217-222.

[13] B. Liu, X. Zhou, T. Hashimoto, X. Zhang, J. Wang, Machining introduced microstructure modification in aluminium alloys, J. Alloy. Compd. 757 (2018) 233-238.

[14] J. Wang, X. Zhou, G.E. Thompson, J.A. Hunter, Y. Yuan, Delamination of near-surface layer on cold rolled AlFeSi alloy during sheet forming, Mater. Charact. 99 (2015) 109-117.

[15] M. Fishkis, J.C. Lin, Formation and evolution of a subsurface layer in a metalworking process, Wear 206 (1997) 156-170.

[16] K. Li, X. Zhou, G.E. Thompson, J.A. Hunter, Y. Yuan, Evolution of near-surface deformed layers on AA3104 aluminium alloy, Mater. Sci. Forum 765 (2013) 358-362.

[17] I. Lindseth, A. Bardal, R. Spooren, Reflectance measurements of aluminium surfaces using integrating spheres, Opt. Lasers Eng. 32 (1999) 419–435. doi:10.1016/S0143-8166(00)00010-5.

[18] Premandra, J.H. Chen, F.D. Tichelaar, H. Terryn, J.H.W. de Wit, L. Katgerman, Optical and transmission electron microscopical study of the evolution of surface layer on recycled aluminium along the rolling mills, Surf. Coatings Technol. 201 (2007) 4561–4570. doi:10.1016/j.surfcoat.2006.09.090.

[19] M.I. Abd El Aal, N. El Mahallawy, F.A. Shehata, M. Abd El Hameed, E.Y. Yoon, H.S. Kim, Wear properties of ECAP-processed ultrafine grained Al-Cu alloys, Mater. Sci. Eng. A. 527 (2010) 3726–3732. doi:10.1016/j.msea.2010.03.057.

[20] N. Gao, C.T. Wang, R.J.K. Wood, T.G. Langdon, Tribological properties of ultrafine-grained materials processed by severe plastic deformation, J. Mater. Sci. 47 (2012) 4779–4797. doi:10.1007/s10853-011-6231-z.

[21] H. Leth-Olsen, A. Afseth, K. Nisancioglu, Filiform corrosion of aluminium sheet. II. Electrochemical and corrosion behaviour of bare substrates, Corros. Sci. 40 (1998) 1195–1214. doi:10.1016/S0010-938X(98)00025-0.

[22] H.N. McMurray, A.J. Coleman, G. Williams, A. Afseth, G.M. Scamans, Scanning Kelvin Probe Studies of Filiform Corrosion on Automotive Aluminum Alloy AA6016, J. Electrochem. Soc. 154 (2007) C339. doi:10.1149/1.2731035.

[23] H. Leth-Olsen, J.H. Nordlien, K. Nisancioglu, Filiform corrosion of aluminium sheet. III. Microstructure of reactive surfaces, Corros. Sci. 40 (1998) 2051–2063. doi:10.1016/S0010-938X(98)00094-8.

[24] S. Wang, F. Yang, G.S. Frankel, Effect of Altered Surface Layer on Localized Corrosion of Aluminum Alloy 2024, J. Electrochem. Soc. 164 (2017) C317–C323. doi:10.1149/2.1541706jes.

[25] C. Montero-Ocampo, L. Veleva, Effect of cold reduction on corrosion of carbon steel in aerated 3% sodium chloride, Corrosion 58 (2002) 601-607.

[26] M.A. McMahon, A. Green, K.G. Watkins, W.M. Steen, Effect of residual stress on the corrosion properties of CO2 laser surface melted alloys, Mater. Sci. Forum 192 (1995) 789-796.

[27] X. Zhou, C. Luo, Y. Ma, T. Hashimoto, G.E. Thompson, A.E. Hughes, P. Skeldon, Grain-stored energy and the propagation of intergranular corrosion in AA2xxx aluminium alloys, Surf. Interface Anal. 45 (2013) 1543-1547.

[28] J.C. Aurich, D. Dornfeld, P.J. Arrazola, V. Franke, L. Leitz, S. Min, Burrs-Analysis, control and removal, CIRP Ann. - Manuf. Technol. 58 (2009) 519–542. doi:10.1016/j.cirp.2009.09.004.

[29] B. Mingo, R. Arrabal, A. Pardo, E. Matykina, P. Skeldon, 3D study of intermetallics and their effect on the corrosion morphology of rheocast aluminium alloy, Mater. Charact. 112 (2016) 122–128. doi:10.1016/j.matchar.2015.12.006.

[30] F.J. Humphreys, M. Hatherly, Recrystallization and Related Annealing Phenomena, Manchester, 1995.

[31] C. Luo, X. Zhou, G.E. Thompson, A.E. Hughes, Observations of intergranular corrosion in AA2024-T351: The influence of grain stored energy, Corros. Sci. 61 (2012) 35–44. doi:10.1016/j.corsci.2012.04.005.